ARTICLE

Design Strategy of Infrared 4-Hydroxybenzylidene-imidazolinone-Type Chromophores based on Intramolecular Charge Transfer: a Theoretical Perspective

Jian Song[a*], WenLong Liang[a], Shouning Yang[b], Huayan Yang[b*]

a. School of Physics, Henan Normal University, Xinxiang 453007, China
b. NMPA Key Laboratory for Research and Evaluation of Innovative Drug, Henan Key Laboratory of Organic Functional Molecule and Drug Innovation, Collaborative Innovation Center of Henan Province for Green Manufacturing of Fine Chemicals, School of Chemistry and Chemical Engineering, Henan Normal University, Xinxiang 453007, China

(Dated: Received on October 28, 2022; Accepted on December 6, 2022)

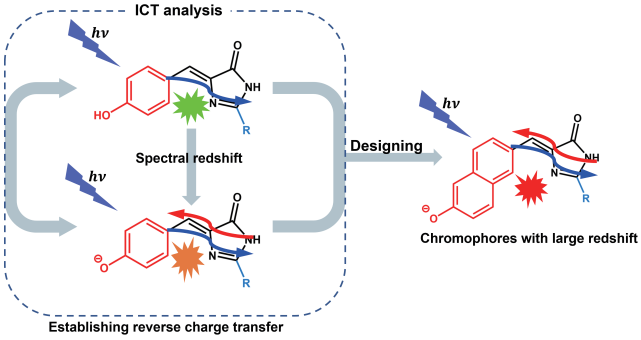

Partial genetically encoded 4-hydroxybenzylidene-imidazolinone (HBI)-type chromophores are new promising fluorescent probes, which are suitable for imaging and detection of living cells. However, the lack of infrared chromophores hinders the development seriously. Here more than 30 HBI-type chromophores with regular structure modifications were employed and typical spectral redshift change laws and mechanisms were investigated by quantum methods. Results show that both one-photon spectrum (OPS, absorption/emission) and two-photon absorption (TPA) can achieve large redshift via either extending conjugated lengths of frag-3 or enlarging conjugated areas of frag-1 of HBI skeleton. Spectral redshifts of all chromophores are highly related to intramolecular charge transfer (ICT), but neutral ones are closely related to the total ICT or electron-accepting-numbers of frag-3, and the high correlative factor of anions is the aromaticity of frag-2 bridge. The frag-2 bridge with high aromaticity can open a reverse charge transfer channel in anion relative to neutral, obtaining significant redshift. Based on analysis, a new 6-hydroxylnaphthalene-imidazolinone (HNI) series, which have larger conjugated area in frag-1, are predicted. The OPS and TPA of anionic HNI ones acquire about 76−96 nm and 119−146 nm redshift relative to traditional HBI series respectively as a whole. The longest emission of anionic HNI-4 realizes more 244 nm redshift relative to HBI-1. Our work clarifies worthy spectral regularities and redshift mechanisms of HBI-type chromophores and provides valuable design strategy for infrared chromophores synthesis in experiment.

Key words: Intramolecular charge transfer, Near-infrared fluorescent chromophore, 4-Hydroxybenzylidene-imidazolinone, One-photon spectrum, Two-photon absorption

I. INTRODUCTION

Near-infrared (NIR) fluorescence imaging is a powerful technology in the imaging of proteins, cells, and tumors, because it has the advantages of deep tissue-penetration, high signal-to-noise ratio and high spatial-temporal resolution [1−4]. The key driving force of NIR fluorescence imaging technology is the development of NIR fluorescent probes. The often-used NIR fluorescent probes, such as BODIPY, cyanine dyes, rho-

* Authors to whom correspondence should be addressed. E-mail: songjian@htu.edu.cn, yanghuayan@htu.edu.cn

damine, are exogenous fluorescent probes, and poor biocompatibility is their common weakness [5–10]. Endogenous probes, such as genetically encoded fluorescent protein (FP), are expected for their special build-in advantages. However, the development of NIR FP probes is still not satisfactory for various reasons [11–13].

Recently, chromophores in the middle of FPs have attracted world-wide attention. 4-Hydroxybenzylideneimidazolinone (HBI) (FIG. 1, HBI-1), the chromophore of green fluorescent protein (GFP), has been commonly shared as the central skeleton of chromophores in most newly developed FPs [13–17]. Conventional wisdom holds that HBI analogue chromophores cannot emit fluorescence independent of their protein cavity. The reason is that the rapid nonradiative decay via the twist of unsupported molecular skeleton will lead to the fluorescent quenching. However, recently a number of solutions have emerged to isolate chromophores and turn on their fluorescence. For instance, HBI analogues become highly fluorescent after being chemically locked, substituted by various hosts or limited by scaffold rotation [18–23]. Its fluorescence also can be turned on in high viscosity environment via suppressing the twisting nonradiative decay [24–30]. Thus, they could serve as good fluorescent probes to monitor or report protein aggregates because of the high viscosity of protein environment. Although some artificial HBI-type chromophores were chemically synthesized in Zhang's work for instance [25], all of them retain the main skeleton of HBI. Experiments also show that they seem more suitable for detection in living cells than traditional chemical probes. That is the reason why they are called partially encoded chromophores. Compared with FPs, they can better distinguish between misfolded oligomers and insoluble aggregates in complex cells [25]. However, up to now, the design of HBI-type probes with NIR fluorescence is still in progress. Designing HBI-type chromophores with longer wavelengths can be inspired by their parent FPs. Large numbers of colorful FPs are obtained by mutating the amino acids surrounding the HBI chromophore in the center of the barrel-like protein. Another strategy that allows the excitation wavelengths of fluorophores to rapidly enter the IR region is the two-photon absorption (TPA) [31, 32]. In the present work, a series of HBI-type chromophores with regular modifications are employed and their structure-spectral properties, both one-photon spectrum (OPS) and TPA, are investigated systematically. High correlation factors between spectral redshifts and typical intramolecular charge transfer (ICT) parameters of neutral chromophores and anionic chromophores are explored. Based on those guidances, a new series of HBI-type chromophores with large redshift relative to HBI are predicted in the end.

II. MODELS, THEORY AND METHODOLOGY

A. HBI/HQI analogue structure models

FIG. 1 demonstrates two series of chromophores from homologous proteins with regular spectral properties, these chromophores in each row have the same molecular skeleton, except the right terminal side chains (blue, frag-3). The difference between the two series is the left conjugated ring, HBI series with phenol ring and 8-hydroxyquinoline-imidazolinone (HQI) series with 8-hydroxyquinoline ring, and they are labeled as HBI-X or HQI-X (X = 1–5) respectively. For HBI series, by replacing the NH_2 group of sfGFP's chromophores (HBI-1) with dihydrooxazole ring (mOFP, HBI-2) or C=O group (asFP, HBI-3), the origin protein's one-photon spectra are significantly red-shifted by adding one double-bond to the frag-3 [14–16]. The substituents of HBI-4 and HBI-5 are *N*-ethylideneformamide group and oxazolone group, both of which possess two double bonds and achieve stronger spectral red shifts in their original FPs, eqFP (HBI-4) and PSmOFP (HBI-5) [13, 17]. The HQI series chromophores are obtained by substituting the phenol ring of HBI-X with an 8-hydroxyquinoline group, and about 30 nm red-shift occurs between their original FPs [33]. It is noted that HQI-3 and HQI-5 are theoretical supplements here, and have not been reported in experiment. Additionally, all the reported HBI-type FPs have two forms in experiment, neutral form and anionic form [34]. The latter is obtained by deprotonating the hydroxyl group of phenol ring or 8-hydroxyquinoline ring, and then the integral molecule is negatively charged. Since the experimental spectra are mixtures of two forms, both neutral and anionic forms of all the HBI and HQI chromophores will be investigated here, with the total number of molecules up to 20. For convenience of description, each chromophore in FIG. 1 is divided into three parts, fragment 1 (frag-1, red colored), fragment 2 (frag-2, black colored) and fragment 3 (frag-3, blue colored).

DOI: 10.1063/1674-0068/cjcp2210157

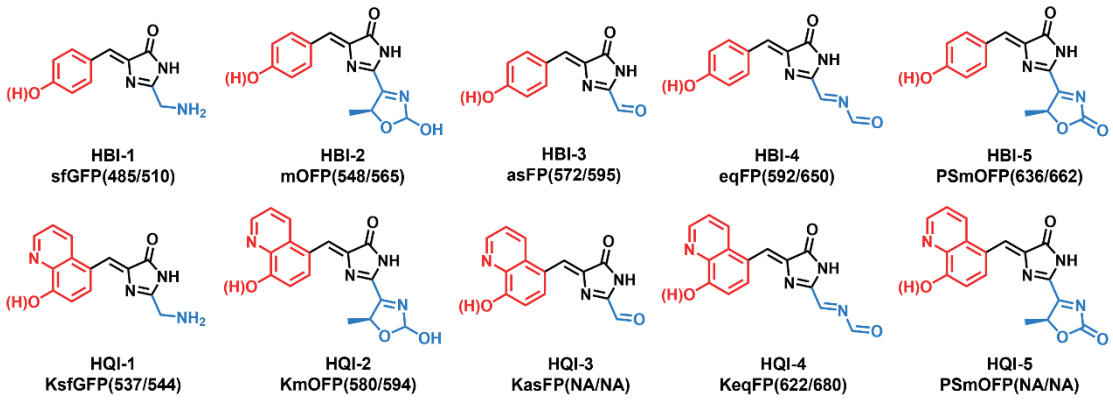

FIG. 1 Two series of HBI-type chromophores: 4-hydroxybenzylidene-imidazolinone (HBI) series (top row) and 8-hydroxyquinoline-imidazolinone (HQI) series (bottom row). The invariant parts of structure are colored in black (labeled as frag-2), variant parts are colored in red (labeled as frag-1) and blue (labeled as frag-3,) respectively. Experimental absorption/emission wavelengths (nm) of their original fluorescent proteins are provided in parentheses. It is noted that the HQI-3 and HQI-5 chromophores have no corresponding fluorescent proteins. Experimental references can be found in Supplementary materials (SM).

B. Quantum methods for OPS and TPA calculations

Both one-photon spectra (OPS) and two-photon absorption (TPA) of all chromophores (neutral and anionic) are calculated using quantum methods. Compared with demanding high-precision methods, such as couple-cluster (CC) and multi-reference methods, TDDFT with proper functionals is a good choice to balance the efficiency and accuracy in excited energy calculations when the number of molecules is large. However, the inborn defect of TDDFT determines its results depending on functionals significantly. The traditional B3LYP functional cannot successfully deal with the excited states of molecules with long-range charge-transfer (CT), Rydberg excitation, and high conjugated/delocalization [35–37]. Some meta-GGA functionals, such as CAM-B3LYP, ω-B97XD with the long-range Hartree-Fock (HF) correlation correction or/and dispersion effects, have been proven to perform well in many HBI analogues' spectra simulations [38–40]. Both the CAM-B3LYP and ω-B97XD functionals were employed to calculate the vertical absorption and emission spectra of chromophores and results (FIG. S1 in Supplementary materials (SM)) show that both of them can arrive at a good consistency between theoretical spectral regularity and experiments.

Compared with OPS, calculation of TPA cross section is more difficult and expensive. Studies have shown CC2 method is a reliable methodology for TPA cross section calculations for FPs' chromophores, as well as for other small- and medium-sized organic molecules [41–44]. The disadvantage of CC2 is expensive and not suitable for computations of a large number of systems. Grabarek *et al.* assessed one- and two-photon absorption properties of neutral and anionic fluorescent proteins chromophores simulated by TDDFT with different functionals, and suggested that TDDFT/CAM-B3LYP with aug-cc-pVDZ, rather than other methods, can well reproduce results of CC2 in the TPA cross section simulations [39]. In order to unify the calculation functionals, CAM-B3LYP/aug-cc-pVDZ method was employed to calculate TPA of all chromophores with Dalton2016 package [45]. Geometry optimizations, OPS (vertical absorption and emission), Mulliken population analysis for each chromophore was obtained with CAM-B3LYP/6-311G(d,p) on Gaussian16 package [46].

C. Intramolecular charge transfer performance analysis

Interfragment charge transfer (IFCT) method is a method to analyze net electron transfer between different fragments of system during excitation based on excited state wavefunction, here Multiwfn package were employed to analyze fragment–fragment charge transfer of chromophores. In IFCT, the interfragment charge transfer matrix (Q) from one fragment of molecule (electron donor, labeled as R) to another fragment of system (electron acceptor, labeled as S) during the excitation is defined as,

$$Q_{\mathrm{R,S}} = \Theta_{\mathrm{R,hole}}\Theta_{\mathrm{S,elec}}$$

Where, $\Theta_{\mathrm{R,hole}}$ and $\Theta_{\mathrm{S,elec}}$ denote hole contribution of fragment R and electron contribution of fragment S during excitation, respectively. Then, the net electron transferred from fragments S to fragment R is

DOI: 10.1063/1674-0068/cjcp2210157

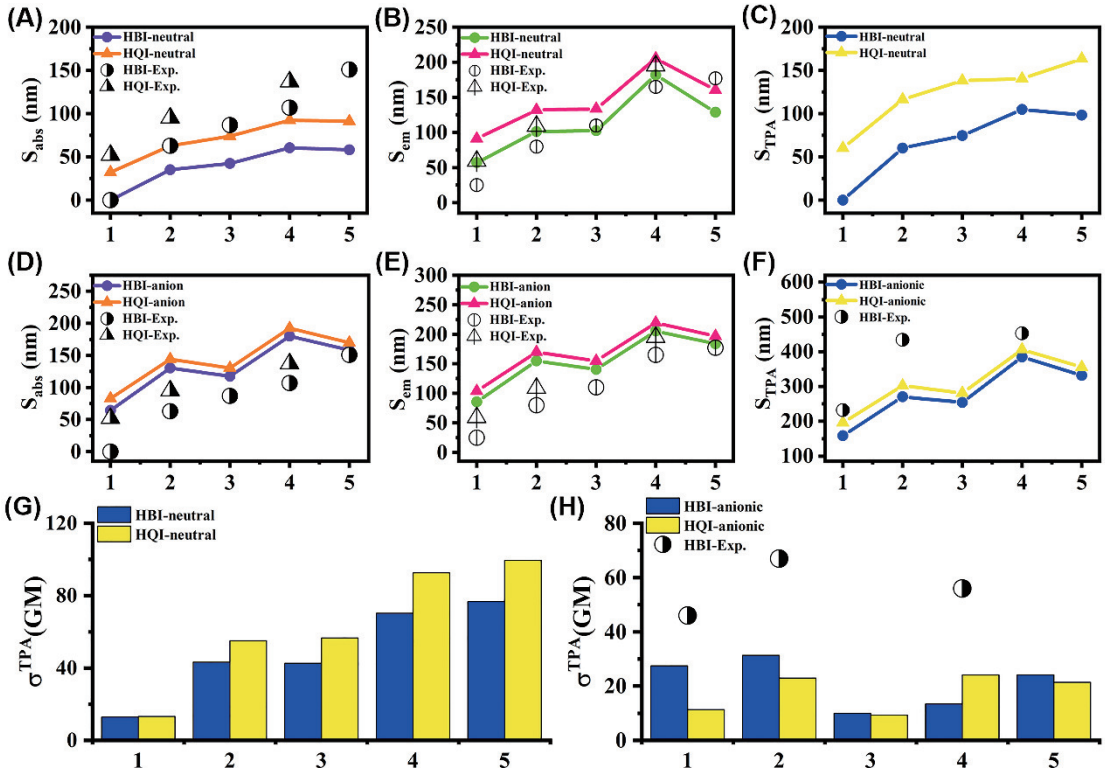

FIG. 2 One-photon spectra (OPS) and two-photon absorption (TPA) spectral patterns of all chromophores in both neutral and anionic forms. The reference wavelengths for theory and experiment are the absorption of neutral HBI-1 and absorption of sfGFP respectively. (A), (B), (C), (G) are one-photon absorption (S_{abs}), one-photon emission (S_{em}), two-photon absorption (S_{TPA}) and two-photon absorption cross section (σ^{TPA}) of neutral chromophores in HBI series and HQI series, respectively. (D), (E), (F), (H) show the anionic ones. Numbers of horizontal ordinates represent the X of HBI-X and HQI-X.

$$P_{S,R} = Q_{S,R} - Q_{R,S}$$

In this work, IFCT analysis based on both $S_0 \rightarrow S_1$ excitation (corresponding to absorption) and $S_1 \rightarrow S_0$ excitation (corresponding to emission) were performed on Multiwfn 3.8 package [47, 48].

III. RESULTS AND DISCUSSIONS

A. One-photon spectra and two-photon absorption

Aiming to focus on the spectral red shifts, the vertical absorption spectral wavelength of neutral HBI-1 is used as references (set it to zero). The one-photon absorption, one-photon emission and two-photon absorption of all other chromophores, both their neutral and anionic forms, are obtained by taking the red shift relative to absorption of neutral HBI-1. Here, the one-photon absorption, one-photon emission, two-photon absorption, and two-photon absorption cross section are labeled as S_{abs}, S_{em}, S_{TPA}, and σ^{TPA} respectively. The experimental reference value is the absorption wavelength of the superfolder green fluorescent protein (sfGFP), which is a mixture of neutral and anionic FPs. All the spectral shift patterns, as well as their comparisons with experiments, are plotted in FIG. 2 (the detailed data can be found in Tables S1–S3 in SM). As seen, S_{abs}, S_{em}, and S_{TPA} of both neutral and anionic chromophores increase with the numbers of frag-3's double-bond in each series, which is consistent well with experiment. Generally, chromophores with the two double bonds in right terminal groups, such as HBI-4/HBI-5 or HQI-4/HQI-5, present the largest red shifts, and those with single double bond modifications, such as HBI-2/HBI-3 or HQI-2/HQI-3, present a slightly smaller red shift. The substitution of phenol ring (HBI series) by 8-hydroxyquinoline group (HQI series) leads to red shifts overall in both absorption and emission. All these spectral regularities are in good agreement with the experiment. Results further suggest that the red shift degree of S_{em} from HBI-1 (HQI-1) to HBI-4/HBI-5 (HQI-4/HQI-5) is bigger than that of S_{abs} in the same series of like charges. The red shift degree in series of negative charges (anionic series) is bigger than that in neutral series. For instance, S_{abs} of HBI-4/HBI-5 are 58/60 nm

DOI: 10.1063/1674-0068/cjcp2210157

(neutral) and 94/116 nm (anionic), and the experimental data are 107/151 nm. The increases of S_{abs} from HQI-1 to HQI-4/HQI-5 are 59/60 nm (neutral) and 87/109 nm (anionic), close to 85 nm in experiment. The S_{em} of HBI-4/HBI-5 are 72/125 nm (neutral) and 98/120 nm (anionic) and the experiment value is 140/152 nm. The S_{em} shifts from HQI-1 to HQI-4/HQI-5 are 69/114 nm (neutral) and 93/115 nm (anionic), matching well with experiment value of 136 nm. The whole red shift of both S_{abs} from HBI series to HQI series is 24−34 nm, which is consistent well with 30 nm in experiment. The difference between anionic chromophore and neutral one is further widened with the increase of the number of double-bond in frag-3. For example, the S_{abs} of anionic HBI-1 about 64 nm red shifts than that of neutral HBI-1, and those values are up to 180 nm and 159 nm for the absorption of HBI-4 and HBI-5 respectively. It is noted that the theoretical spectral orders between HBI-4 and HBI-5 or between HBI-2 and HBI-3 in some spectral cases, such as anionic S_{abs}, neutral S_{em} and anionic S_{em}, are different from experiment. These differences are more likely to be attributed to the protein environments, because it has been widely proven by previous studies that the protein environments of chromophores can result in either red shift or blue shift of spectra in FPs [13, 49].

The S_{TPA} and TPA cross sections (σ^{TPA}) of all chromophores are also summarized in FIG. 2. The S_{TPA} values of all chromophores have significant red shifts relative to neutral HBI-1, and their change rules are similar to those of their OPS. For example, with the increase in the number of double bonds in frag-3, the S_{TPA} values of both HBI and HQI series raise remarkably. The anionic chromophore has larger S_{TPA} than its neutral one, and the S_{TPA} values of HQI series are larger than that of HBI series. As a whole, the σ^{TPA} values of neutral chromophores are larger than those of anionic ones. The neutral σ^{TPA} generally increases with the extension of conjugated bonds of frag-3 in each row, but this is not always true in anions. In anions, the σ^{TPA} first increases from HBI-1 to HBI-2 and then decreases, this variation regularity is in good agreement with experiment. After the replacement of HBI by HQI, the difference of σ^{TPA} between two series is slight in both neutral or anionic forms, and both of them share the similar change rule in σ^{TPA}.

B. IFCT and correlations analysis

As well known, spectra changes of fluorophores usually have very close relationship with the changes of intramolecular charge transfer (ICT) [50−54]. HBI-type chromophores are typical ICT systems. Taking HBI-1 as an example, phenol ring acts as an electron-donating role, and charge transfer occurs from phenol ring (frag-1) to alkene-bridged imidazole ring (frag-2) and the right-side chains (frag-3), both of which are electron acceptors. In this section, interfragment charge transfer (IFCT) and correlations analysis are investigated, aiming to clarify the relationship law between spectral behaviors and ICT features, which are caused by structure modifications. All compounds in FIG. 1 are divided into three fragments, frag-1 (red), frag-2 (black) and frag-3 (blue). IFCT analysis of $S_0 \rightarrow S_1$ (absorption) and $S_1 \rightarrow S_0$ (emission) excitations, and important correlation analysis are summarized in FIG. 3 (neutral) and FIG. 4 (anionic). Results show that the spectra changes of neutral chromophores and anionic chromophores with structure modifications are not the same. They demonstrate different ICT features and their different highly-correlated factors of spectral red shift, in OPS or TPA, are given here. For clarity, neutral and anionic forms would be discussed respectively.

As show in FIG. 3, the ICT is observed in both HBI and HQI series in the neutral forms. With the increase of double bond in frag-3, more electrons are transferred from frag-1 to frag-2 and/or frag-3, and their ICT are enhanced. For instance, the total charge transfer numbers (N_{total}) of HBI-2/HBI-3 and HBI-4/HBI-5 increase by about 0.08−0.1 e and 0.12 e relative to HBI-1 respectively during the absorption excitations ($S_0 \rightarrow S_1$). The electron-accepting numbers of frag-3 ($N_{frag\text{-}3}$) rise from −0.01 e (HBI-1) up to −0.27 e (HBI-4/HBI-5) in HBI series. Similar N_{total} and $N_{frag\text{-}3}$ regularities are found during the emission processes ($S_1 \rightarrow S_0$), although fluctuations exist. Correlation analysis show that the spectral shift behaviors of S_{abs}, S_{em}, and S_{TPA} do demonstrate high correlations with N_{total} and $N_{frag\text{-}3}$ in both HBI and HQI series. All their correlation coefficients (R^2) are above 0.909 and most R^2 are in 0.98 − 1.0. Unlike the spectral wavelengths, the cross sections σ^{TPA} seem to demonstrate high correlation only to N_{total}, the R^2 values of HBI and HQI series are 0.821 and 0.858, respectively. When the phenol ring (HBI series) is replaced by hydroxyquinoline (HQI series), more electrons transfer from frag-1 ($N_{frag\text{-}1}$) to frag-2 isobserved. This could be attributed to the larger π structure of hydroxyquinoline than phenol ring in frag-

DOI: 10.1063/1674-0068/cjcp2210157

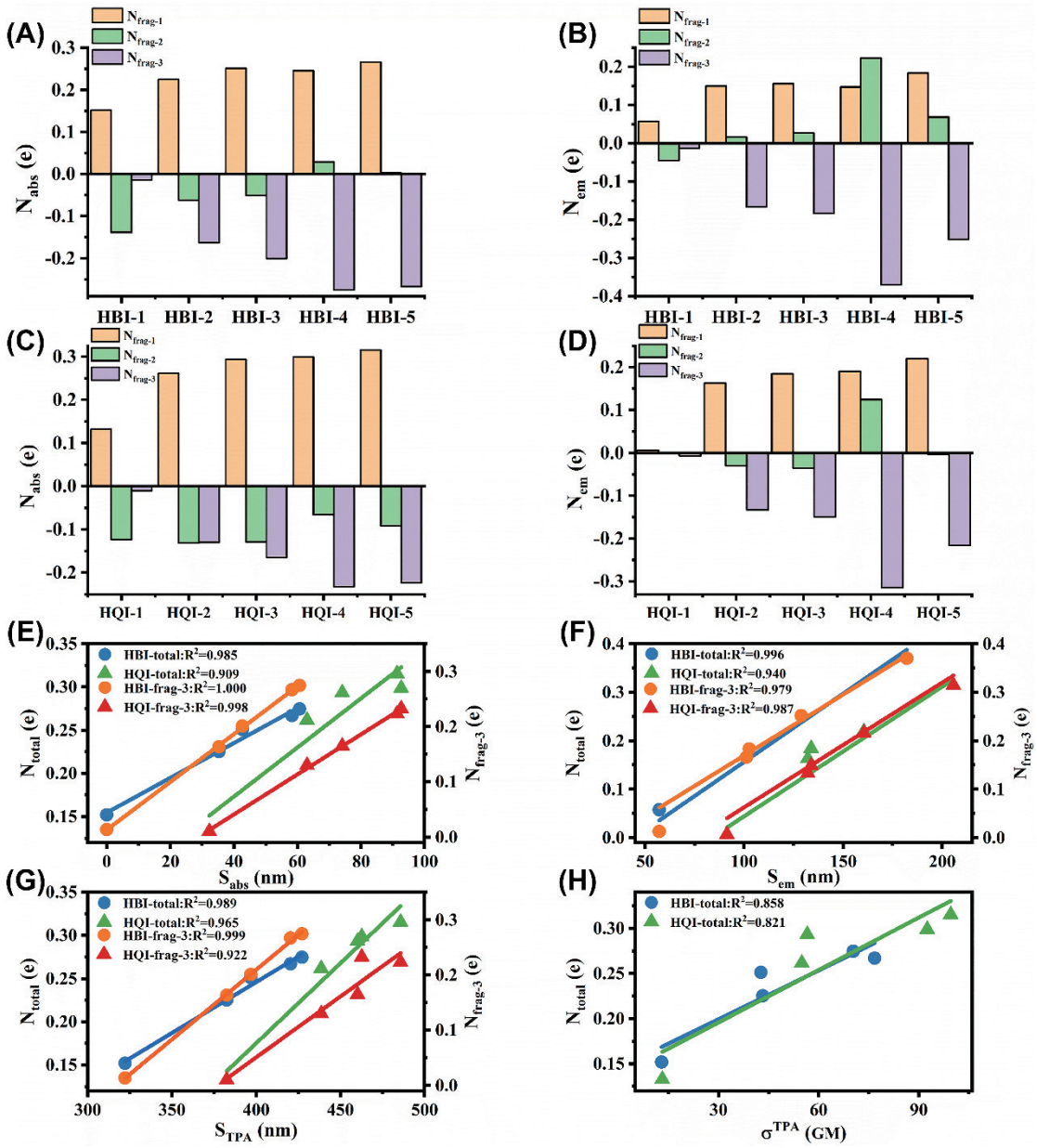

FIG. 3 Interfragment charge transfer (IFCT) of absorption (A, C) and emission (B, D) of neutral HBI and HQI series and corresponding correlations analysis with S_{abs} (E), S_{em} (F), S_{TPA} (G), and σ^{TPA} (H). The N_{abs} and N_{em} are the numbers of losing (positive) or gaining (negative) electrons of different fragment in OPS absorption and emission, respectively. N_{total} and $N_{frag\text{-}3}$ are the total electron number of molecular ICT and the number of gaining electrons of frag-3, respectively.

1. Highly and largely conjugated structure of hydroxyquinoline makes HQI-series chromophores have more transferable or free electrons than chromophore in HBI series, resulting in an overall red shift of HQI series when compared with HBI series.

After deprotonation, the IFCT of those anionic chromophores changes quite differently from that of the neutral ones. Although frag-3 is still a good electron acceptor, the electron-donating abilities of frag-1 are gradually weakened and the role of frag-2 shift from electron acceptors to electron donors along with the conjugated extension of frag-3 in those anionic chromophores. Taking HBI-4 as an example, the frag-1 together with frag-3 receives electrons from frag-2 and a brand-new charge transfer channel, from middle to both ends, is built. Correlation analysis show that S_{abs}, S_{em}, and S_{TPA} behaviors of anionic chromophores seem more related to charge transfer numbers of frag-2 ($N_{frag\text{-}2}$), instead of N_{total} or $N_{frag\text{-}3}$. The correlative factors (R^2) of S_{abs}, S_{em}, and S_{TPA} with $N_{frag\text{-}2}$, are in the range of

DOI: 10.1063/1674-0068/cjcp2210157

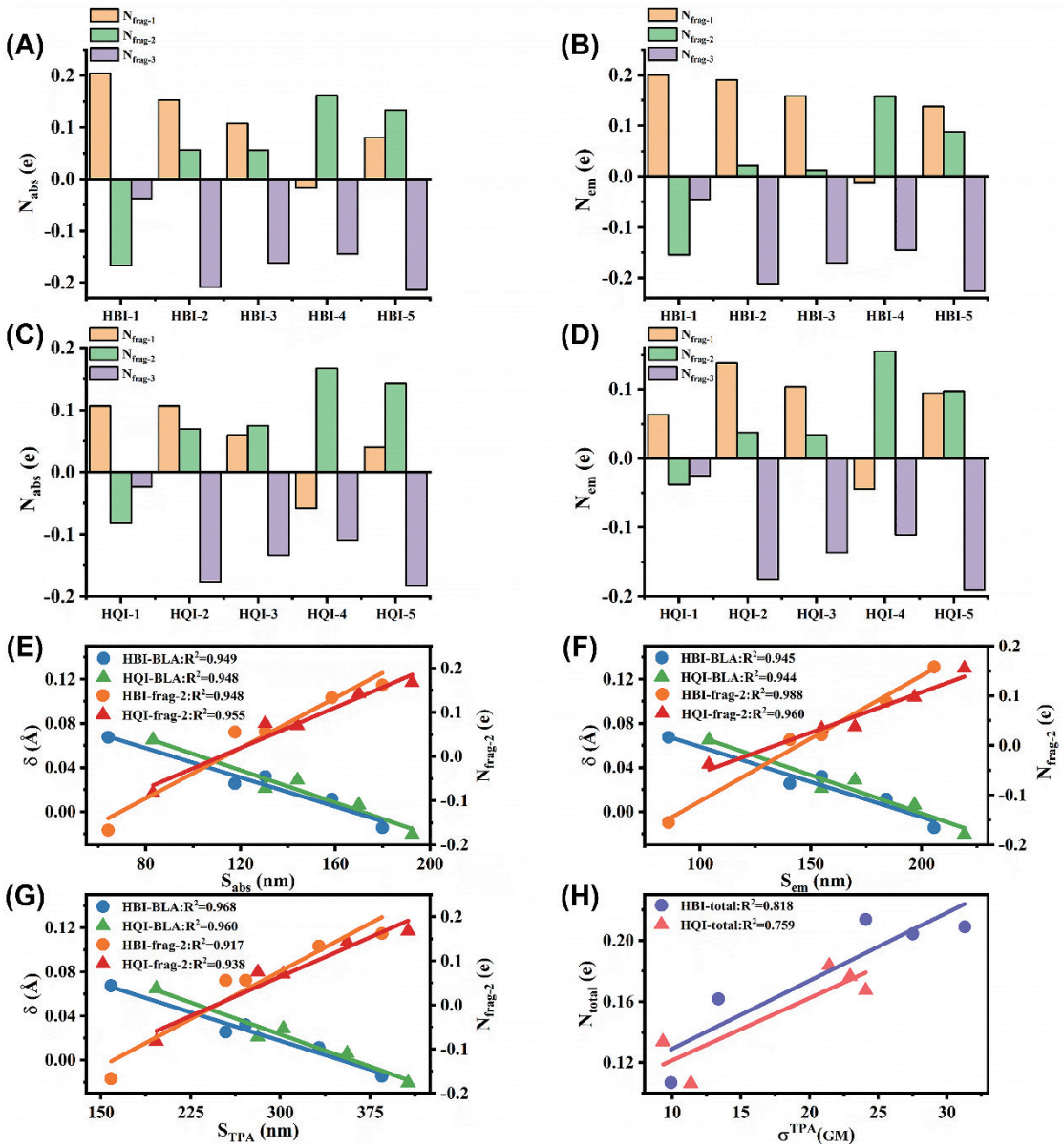

FIG. 4 Interfragment charge transfer (IFCT) of absorption (A, C) and emission (B, D) of anionic HBI and HQI series and corresponding correlations analysis with $S_{\rm abs}$ (E), $S_{\rm em}$ (F), $S_{\rm TPA}$ (G), and $\sigma^{\rm TPA}$ (H). The $N_{\rm abs}$ and $N_{\rm em}$ are the numbers of losing (positive) or gaining (negative) electrons of different fragment in OPS absorption and emission respectively. δ is the bond length alternation of frag-2, $N_{\rm total}$ and $N_{\rm frag\text{-}2}$ are the total electron number of molecular ICT and the number of gaining electrons of frag-2 respectively.

0.917–0.988. Only the $\sigma^{\rm TPA}$ still keeps in a good correlation with $N_{\rm total}$ because $\sigma^{\rm TPA}$ is related to both transition dipole moment ($\mu_{\rm if}$) and permanent dipole moment change ($\Delta\mu$), which have close relationship with ICT. To find out why $N_{\rm frag\text{-}2}$ has so high correlation with spectral redshift, the bond length alternation (BLA, labeled as δ, the detailed description can be found in Text S1 in SM), which is defined as the difference between the average values of long and short carbon-carbo; on bonds in conjugated molecules, is calculated for all chromophores in ground states. The small or zero BLA indicates a high aromaticity or π-electron delocalization, on the contrary, large BLA indicates π-electron localization or the absence of aromaticity [55]. Results in FIG. 5 show that the frag-2 changes from a weak aromatic group in HBI-1 to a stronger aromatic group in HBI-4/HBI-5 along with the double bonds increase of frag-3. This is a good explanation for the role transition of frag-2, from an electron-acceptor in HBI-1 to a strong electron-donating group in HBI-4/HBI-5. The correlative factors (FIG. 4) between aromaticity of frag-2 and spectral shifts (including $S_{\rm abs}$, $S_{\rm em}$, $S_{\rm TPA}$)

DOI: 10.1063/1674-0068/cjcp2210157

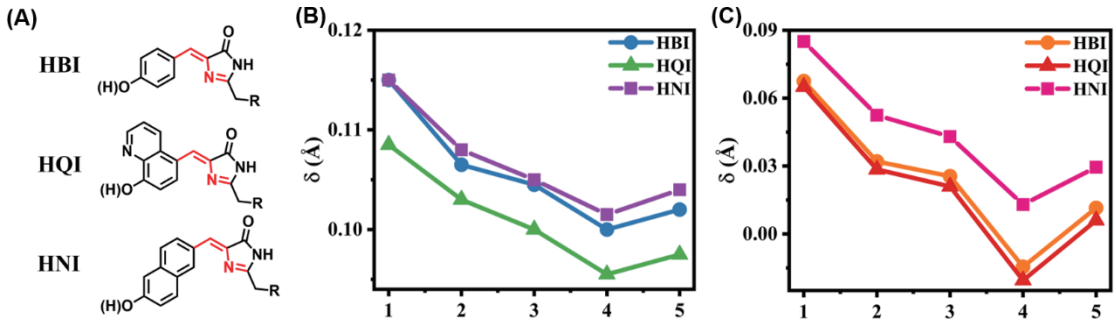

FIG. 5 Comparison of BLA values of frag-2 of different series. (A) Structures of HBI, HQI, 6-hydroxyl-naphthalene-imidazolinone (HNI). Red bonds in frag-2 are carbon-carbon bonds for BLA calculation. (B) BLA values (δ) of neutral HBI, HQI, and HNI series. (C) BLA values (δ) of anionic HBI, HQI, and HNI series. HNI: 6-hydroxyl-naphthalene-imidazolinone, BLA: the bond length alternation.

are 0.945−0.968, indicating a high correlation between them. It seems that the two-double-bond structures in frag-3 of HBI-4/HBI-5 induce a high π-conjugated feature of frag-2, endowing frag-2 with strong electron-donating ability. The frag-2 section of HBI-4, which has the highest aromaticity in all compounds, acts as an electron donor independently and two CT channels, from frag-2 to frag-1 and from frag-2 to frag-3, are built. The direction of the former channel from frag-2 to frag-1 is totally opposite to that of ICT in neutral HBI-4. Correspondingly, the anionic HBI-4 presents the largest spectral red shift ($S_{\rm abs}$, $S_{\rm em}$, $S_{\rm TPA}$) of the whole HBI series. With the replacement of phenol ring by hydroxyquinoline, the aromaticity of frag-2 is further enhanced and the related coefficients between aromaticity of frag-2 and spectral shifts ($S_{\rm abs}$, $S_{\rm em}$, $S_{\rm TPA}$) are still very high (0.944−0.960). It is suggested that larger conjugation of frag-1 can offer more π-electrons, which further improve the aromaticity of frag-2 and reduce the roughness of charge transfer road. The neutral HQI-4 provides the largest ICT from frag-1 and frag-2 to frag-3 in emission process, in contrast, the anionic HQI-4 demonstrates the strongest two-direction CT channel, from frag-2 to frag-1 and from frag-2 to frag-3. In addition, the lower δ of frag-2 anionic chromophore may explain the longer spectral shifts ($S_{\rm abs}$, $S_{\rm em}$, $S_{\rm TPA}$) of anionic chromophore when compared to its neutral one. From the BLA of frag-2 in FIG. 5, it is also found that when $\delta \leq 0.1$ Å, the reverse charge transfer channel from frag-2 to frag-1 is opened and two-direct CT channel is set up, resulting in large spectral shifts.

C. Predicted chromophore with large redshift

The most common design strategies of chromophores with large spectral red shift include introducing or enhancing ICT of molecules by different electron-donating/withdrawing substitution, extending conjugated length or area of system *etc.* [52, 56−58]. From the above studies, it can be seen that increasing the double bonds of frag-3 can effectively strengthen the ICT of chromophores, resulting in regular spectral red shifts in the same series. Meanwhile, the substitution of the phenol ring by the polycyclic hydroxyquinoline raises the spectral red shifts of chromophore series as a whole. IFCT and correlation analysis prompts that spectral shifts of neutral and anionic HBI-type chromophores possess different high correlation factors. The former is highly associated with total numbers of ICT and electron-accepting numbers of frag-3, and the related factors of the latter is the aromaticity of frag-2. It is noteworthy that both of them can be effectively improved by increasing the conjugated degree of frag-1, such as hydroxyquinoline substitution. Here, we keep the frag-2 and frag-3 unchanged and replace the hydroxyquinoline of HQI series by hydroxyl-naphthalene ring. The purpose is to eliminate the possible electronic localization induced by the nitrogen atom in quinoline, releasing more transferable π-electrons in ICT. All the predicted chromophores are shown in FIG. 6 and they are named as 6-hydroxyl-naphthalene-imidazolinone (HNI) series.

As seen in FIG. 6, the spectral patterns of $S_{\rm abs}$, $S_{\rm em}$, $S_{\rm TPA}$ and $\sigma^{\rm TPA}$ in HNI series have similar behaviors to HBI series or HQI series as expected. The $S_{\rm abs}$, $S_{\rm em}$, $S_{\rm TPA}$ of neutral HNI series do not show much advantage over those of neutral HQI series, or even smaller in some cases. However, spectra shift of anionic HNI series overtake those of all anions. The $S_{\rm em}$ of anionic HNI series have a red shift of about 76−96 nm red shift relative to those of HBI series, which is well above the ~30 nm red shift of HQI series. The anionic $S_{\rm TPA}$ of HNI series achieve a red shif of about 119−146 nm relative to HBI series (the values of HQI series are only

DOI: 10.1063/1674-0068/cjcp2210157

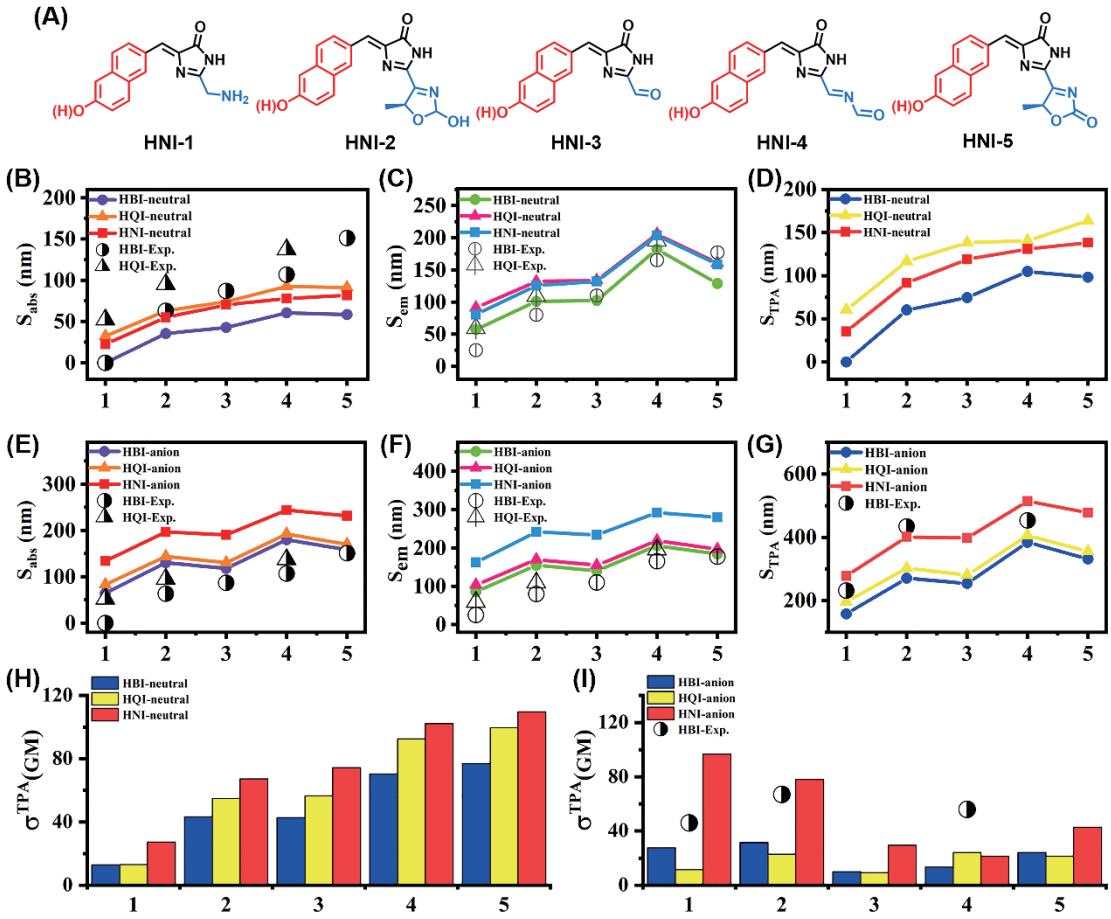

FIG. 6 The predicted HNI series and the comparison with other series in OPS and TPA. (A) Structures of HNI series. (B), (C), (D), (H) are S_{abs}, S_{em}, S_{TPA}, and σ^{TPA} of neutral series respectively. (E), (F), (G), (I) are S_{abs}, S_{em}, S_{TPA}, and σ^{TPA} of anionic series respectively.

22−38 nm). Particularly, the S_{em} of anionic HNI-4 is up to 292 nm relative to neutral HBI-1 absorption and nearly 72 nm higher than the previous S_{em} of anionic HQI-4. The σ^{TPA} of HNI series are also enlarged in both neutral and anion forms. The IFCT results show that the number of charge transfer, both total ICT numbers or partial electron losing or gaining numbers, has been comprehensively increased in HNI series (FIG. S5 in SM). The reason is that the large conjugated area of frag-1 (naphthalene ring) in HNI series can offer the most conjugated electrons of three series. As seen in FIG. 5 and FIG. 6, the aromaticity order of three series is not consistent with the order of their spectral redshift. Specifically, in neutral forms, the aromaticity order is HQI series > HBI series ≈ HNI series (FIG. 5). However, the general order of their spectral redshifts is HNI series ≈ HQI series > HBI series (FIG. 6). In anionic chromphores, the aromaticity order is HQI series ≈ HBI series > HNI series (FIG. 5), but the order of spectral redshift is HNI series >> HQI series > HBI series (FIG. 6). On a whole, the predicted HNI series, which is not dominant in aromaticity, still obtain large spectral redshifts, especially in anionic forms. There are two aspects on the reasons to discuss, which are the maximum number of conjugated area offered in HNI series and the BLA values. We speculate that BLA=0.1 Å is probably a critical threshold value. When the BLA value is less than 0.1 Å, the aromaticity of system is high enough that it dose not hinder the movement of conjugated electrons, and it can even act as an electron donor role. Although the aromaticity of anionic HNI series decrease, its BLA value is still less than 0.1 Å, which indicates that the aromaticity of anionic HNI series is very high. Combined with the richest conjugated electrons, it is easy for HNI series to achieve the largest spectral redshift.

IV. CONCLUSION

In this work, the spectral redshift properties and

DOI: 10.1063/1674-0068/cjcp2210157

mechanisms in both OPS and TPA of up to 30 HBI-type chromophores are investigated. Results demonstrate totally different underlying redshift mechanisms between neutral and anionic chromophores. Besides traditional conjugate extension or substitution with electron withdrawing/donating abilities at the end group, the aromaticity of intermediate bridge (frag-2) should also be concerned. Our results indicate the frag-2 bridge with high aromaticity can pave a smooth way for ICT, achieving significant spectral redshift in both absorption and emission. New series, which have larger conjugated area in frag-1, are predicted and large spectral redshifts relative to reported series are obtained in their anionic forms. Although the stability of the new chromophore series needs to be further tested in the laboratory, it is believed that our work provides valuable design strategy and candidates for the development of NIR HBI-type chromophores.

Supplementary materials: Detailed introduction about bond length abenchmark of OPS computational protocol and IFCT analysis of all chromophores are available. Table S1, Table S2–S4 and Table S5–S6 present experimental references of original protein chromophores, spectral data of chromophores and IFCT analysis of all chromophores mentioned in this work.

V. ACKNOWLEDGEMENTS

This work is supported by the National Natural Science Foundation of China (No.U1904196, No.82073699), the Natural Science Foundation of Henan (No.222300420055).

[1] E. Cassette, M. Helle, L. Bezdetnaya, F. Marchal, B. Dubertret, and T. Pons, Adv. Drug Deliv. Rev. **65**, 719 (2013).
[2] J. Klohs, A. Wunder, and K. Licha, Basic Res. Cardiol. **103**, 144 (2008).
[3] K. D. Piatkevich, F. V. Subach, and V. V. Verkhusha, Chem. Soc. Rev. **42**, 3441 (2013).
[4] C. L. Amiot, S. Xu, S. Liang, L. Pan, and J. X. Zhao, Sensors **8**, 3082 (2008).
[5] R. Sang, X. Xu, Q. Wang, Q. Fan, and W. Huang, Acta Chim. Sin. **78**, 901 (2020).
[6] C. Ding, Y. Huang, Z. Shen, and X. Chen, Adv. Mater. **33**, 2007768 (2021).
[7] Z. Chang, F. Liu, L. Wang, M. Deng, C. Zhou, Q. Sun, and J. Chu, Chin. Chem. Lett. **30**, 1856 (2019).
[8] Y. Chen, L. Li, W. Chen, H. Chen, and J. Yin, Chin. Chem. Lett. **30**, 1353 (2019).
[9] L. Chen and H. Han, Microchim. Acta **181**, 1485 (2014).
[10] J. Zhang, H. Ye, Y. Jin, and D. Han, Top. Curr. Chem. **380**, 2972 (2022).
[11] F. V. Subach and V. V. Verkhusha, Chem. Rev. **112**, 4308 (2012).
[12] R. N. Day and M. W. Davidson, Chem. Soc. Rev. **38**, 2887 (2009).
[13] S. Pletnev, N. V. Pletneva, E. A. Souslova, D. M. Chudakov, S. Lukyanov, A. Wlodawer, Z. Dauter, and V. Pletnev, Acta Crystallogr. D **68**, 1088 (2012).
[14] G. M. Olenginski, J. Piacentini, D. R. Harris, N. A. Runko, B. M. Papoutsis, J. R. Alter, K. R. Hess, S. H. Brewer, and C. M. Phillips-Piro, Acta Crystallogr. D **77**, 1010 (2021).
[15] X. K. Shu, N. C. Shaner, C. A. Yarbrough, R. Y. Tsien, and S. J. Remington, Biochemistry **45**, 9639 (2006).
[16] I. V. Yampolsky, S. J. Remington, V. I. Martynov, V. K. Potapov, S. Lukyanov, and K. A. Lukyanov, Biochemistry **44**, 5788 (2005).
[17] O. M. Subach, G. H. Patterson, L. M. Ting, Y. Wang, J. S. Condeelis, and V. V. Verkhusha, Nat. Methods **8**, 771 (2011).
[18] Y. H. Hsu, Y. A. Chen, H. W. Tseng, Z. Y. Zhang, J. Y. Shen, W. T. Chuang, T. C. Lin, C. S. Lee, W. Y. Hung, B. C. Hong, S. H. Liu, and P. T. Chou, J. Am. Chem. Soc. **136**, 11805 (2014).
[19] C. L. Walker, K. A. Lukyanov, I. V. Yampolsky, A. S. Mishin, A. S. Bommarius, A. M. Duraj-Thatte, B. Azizi, L. M. Tolbert, and K. M. Solntsev, Curr. Opin. Chem. Eng. **27**, 64 (2015).
[20] M. Pattabiraman and A. Natarajan, *Photophysicochemical Processes Directed Within Nano-Containers*, Cham: Springer International Publishing, 321 (2020).
[21] A. Baldridge, A. Amador, and L. M. Tolbert, Langmuir **27**, 3271 (2011).
[22] S. R. Samanta, J. P. Da Silva, A. Baldridge, L. M. Tolbert, and V. Ramamurthy, Org. Lett. **16**, 3304 (2014).
[23] A. Singh, S. Karmakar, I. M. Abraham, D. Rambabu, D. Dave, R. Manjithaya, and T. K. Maji, Inorg. Chem. **59**, 8251 (2020).
[24] Y. Liu, C. H. Wolstenholme, G. C. Carter, H. Liu, H. Hu, L. S. Grainger, K. Miao, M. Fares, C. A. Hoelzel, H. P. Yennawar, G. Ning, M. Du, L. Bai, X. Li, and X. Zhang, J. Am. Chem. Soc. **140**, 7381 (2018).
[25] C. H. Wolstenholme, H. Hu, S. Ye, B. E. Funk, D. Jain, C. H. Hsiung, G. Ning, Y. Liu, X. Li, and X. Zhang, J. Am. Chem. Soc. **142**, 17515 (2020).
[26] K. H. Jung, M. Fares, L. S. Grainger, C. H. Wolstenholme, A. Hou, Y. Liu, and X. Zhang, Org. Biomol. Chem. **17**, 1906 (2019).
[27] A. Saady, V. Böttner, M. Meng, E. Varon, Y. Shav-Tal, C. Ducho, and B. Fischer, Eur. J. Med. Chem. **173**, 99 (2019).

DOI: 10.1063/1674-0068/cjcp2210157

[28] L. Cai, H. Li, X. Yu, L. Wu, X. Wei, T. D. James, and C. Huang, ACS Appl. Bio. Mater. **4**, 2128 (2021).
[29] X. Li, R. Zhao, Y. Wang, and C. Huang, J. Mater. Chem. B **6**, 6592 (2018).
[30] X. Zhi, B. Shen, and Y. Qian, New J. Chem. **44**, 8823 (2020).
[31] Z. Zheng, T. Zhang, H. Liu, Y. Chen, R. T. K. Kwok, C. Ma, P. Zhang, H. H. Y. Sung, I. D. Williams, J. W. Y. Lam, K. S. Wong, and B. Z. Tang, ACS Nano **12**, 8145 (2018).
[32] D. Li, P. Jing, L. Sun, Y. An, X. Shan, X. Lu, D. Zhou, D. Han, D. Shen, Y. Zhai, S. Qu, R. Zboril, and A. L. Rogach, Adv. Mater. **30**, 1705913 (2018).
[33] X. Liu, J. Li, C. Hu, Q. Zhou, W. Zhang, M. Hu, J. Zhou, and J. Wang, Angew. Chem. Int. Ed. **52**, 4805 (2013).
[34] J. Tay, M. A. Parkes, K. Addison, Y. Chan, L. Zhang, H. C. Hailes, P. C. Bulman Page, S. R. Meech, L. Blancafort, and H. H. Fielding, J. Phys. Chem. Lett. **8**, 765 (2017).
[35] A. Nakata, Y. Imamura, and H. Nakai, J. Chem. Phys. **125**, 064109 (2006).
[36] A. Nakata, Y. Imamura, T. Otsuka, and H. Nakai, J. Chem. Phys. **124**, 94105 (2006).
[37] I. Y. Zhang, J. Wu, and X. Xu, Chem. Commun. **46**, 3057 (2010).
[38] X. Chen, J. Song, Z. N. Chen, T. Jin, F. Q. Long, H. Xie, Y. S. Zheng, W. Zhuang, and L. Zhang, J. Comput. Chem. **39**, 2307 (2018).
[39] D. Grabarek and T. Andruniów, J. Chem. Theory Comput. **15**, 490 (2019).
[40] B. Kang, K. Y. Baek, and J. Y. Lee, Bull Korean Chem. Soc. **36**, 276 (2015).
[41] D. H. Friese, C. Hättig, and K. Ruud, Phys. Chem. Chem. Phys. **14**, 1175 (2012).
[42] D. Kánnár and P. G. Szalay, J. Mol. Model. **20**, 2503 (2014).
[43] M. A. Salem and A. Brown, J. Chem. Theroy Comput. **10**, 3260 (2014).
[44] M. Schreiber, M. R. Silva-Junior, S. P. Sauer, and W. Thiel, J. Chem. Phys. **128**, 134110 (2008).
[45] K. Aidas, C. Angeli, K. L. Bak, V. Bakken, R. Bast, L. Boman, O. Christiansen, R. Cimiraglia, S. Coriani, P. Dahle, E. K. Dalskov, U. Ekström, T. Enevoldsen, J. J. Eriksen, P. Ettenhuber, B. Fernández, L. Ferrighi, H. Fliegl, L. Frediani, K. Hald, A. Halkier, C. Hättig, H. Heiberg, T. Helgaker, A. C. Hennum, H. Hettema, E. Hjertenæs, S. Høst, I.-M. Høyvik, M. F. Iozzi, B. Jansík, H. J. A. Jensen, D. Jonsson, P. Jørgensen, J. Kauczor, S. Kirpekar, T. Kjærgaard, W. Klopper, S. Knecht, R. Kobayashi, H. Koch, J. Kongsted, A. Krapp, K. Kristensen, A. Ligabue, O. B. Lutnæs, J. I. Melo, K. V. Mikkelsen, R. H. Myhre, C. Neiss, C. B. Nielsen, P. Norman, J. Olsen, J. M. H. Olsen, A. Osted, M. J. Packer, F. Pawlowski, T. B. Pedersen, P. F. Provasi, S. Reine, Z. Rinkevicius, T. A. Ruden, K. Ruud, V. V. Rybkin, P. Sałek, C. C. M. Samson, A. S. De Merás, T. Saue, S. P. A. Sauer, B. Schimmelpfennig, K. Sneskov, A. H. Steindal, K. O. Sylvester-Hvid, P. R. Taylor, A. M. Teale, E. I. Tellgren, D. P. Tew, A. J. Thorvaldsen, L. Thøgersen, O. Vahtras, M. A. Watson, D. J. D. Wilson, M. Ziolkowski, and H. Ågren, Wires Comput. Mol. Sci. **4**, 269 (2014).
[46] M. J. Frisch, G. W. Trucks, H. B. Schlegel, G. E. Scuseria, M. A. Robb, J. R. Cheeseman, G. Scalmani, V. Barone, G. A. Petersson, H. Nakatsuji, X. Li, M. Caricato, A. V. Marenich, J. Bloino, B. G. Janesko, R. Gomperts, B. Mennucci, H. P. Hratchian, J. V. Ortiz, A. F. Izmaylov, J. L. Sonnenberg, D. Williams-Young, F. Ding, F. Lipparini, F. Egidi, J. Goings, B. Peng, A. Petrone, T. Henderson, D. Ranasinghe, V. G. Zakrzewski, J. Gao, N. Rega, G. Zheng, W. Liang, M. Hada, M. Ehara, K. Toyota, R. Fukuda, J. Hasegawa, M. Ishida, T. Nakajima, Y. Honda, O. Kitao, H. Nakai, T. Vreven, K. Throssell, J. A. Montgomery, Jr., J. E. Peralta, F. Ogliaro, M. J. Bearpark, J. J. Heyd, E. N. Brothers, K. N. Kudin, V. N. Staroverov, T. A. Keith, R. Kobayashi, J. Normand, K. Raghavachari, A. P. Rendell, J. C. Burant, S. S. Iyengar, J. Tomasi, M. Cossi, J. M. Millam, M. Klene, C. Adamo, R. Cammi, J. W. Ochterski, R. L. Martin, K. Morokuma, O. Farkas, J. B. Foresman, and D. J. Fox, *Gaussian 16, Revision B.01*, Wallingford, CT: Gaussian, Inc., (2016).
[47] T. Lu and F. Chen, J. Comput. Chem. **33**, 580 (2012).
[48] T. Lu. *Multiwfn Manual, version 3.8(dev), Section 3.21.8*, available at http://sobereva.com/multiwfn.
[49] M. Drobizhev, N. S. Makarov, S. E. Tillo, T. E. Hughes, and A. Rebane, Nat. Methods **8**, 393 (2011).
[50] M. Kojima, H. Hayashi, T. Aotake, S. Ikeda, M. Suzuki, N. Aratani, D. Kuzuhara, and H. Yamada, Chem. Asian J. **10**, 2337 (2015).
[51] L. Cao, L. Zhang, Q. Wei, J. S. Zhang, D. J. Chen, S. Wang, S. J. Su, T. Wang, and Z. Y. Ge, Dyes Pigm. **176**, 108242 (2020).
[52] Y. L. Li, Z. P. Li, Y. Wang, A. Compaan, T. H. Ren, and W. J. Dong, Energy Environ. Sci. **6**, 2907 (2013).
[53] C. Yan, Z. Guo, W. Chi, W. Fu, S. A. A. Abedi, X. Liu, H. Tian, and W. H. Zhu, Nat. Commun. **12**, 3869 (2021).
[54] L. Xu and Q. Zhang, Sci. China Mater. **60**, 1093 (2017).
[55] M. Kertesz, C. H. Choi, and S. J. Yang, Chem. Rev. **105**, 3448 (2005).
[56] Y. X. Guo, G. H. Lu, J. Z. Zhuo, J. Y. Wang, X. Li, and Z. Q. Zhang, J. Mater. Chem. B **6**, 2489 (2018).
[57] D. K. Zhang, V. Martin, I. Garcia-Moreno, A. Costela, M. E. Perez-Ojeda, and Y. Xiao, Phys. Chem. Chem. Phys. **13**, 13026 (2011).
[58] W. Xu, P. Y. Ma, Q. P. Diao, L. B. Xu, X. Liu, Y. Sun, X. H. Wang, and D. Q. Song, Sens. Actuators B Chem. **252**, 86 (2017).

DOI: 10.1063/1674-0068/cjcp2210157